

This is the accepted manuscript made available via CHORUS. The article has been published as:

## Extinction dynamics of spiral defect chaos

David Vidmar and Wouter-Jan Rappel

Phys. Rev. E **99**, 012407 — Published 9 January 2019

DOI: [10.1103/PhysRevE.99.012407](https://doi.org/10.1103/PhysRevE.99.012407)

# Extinction Dynamics of Spiral Defect Chaos

David Vidmar and Wouter-Jan Rappel

*Department of Physics, University of California, San Diego, La Jolla, CA 92093*

## Abstract

Spatially extended excitable systems can exhibit spiral defect chaos (SDC) during which spiral waves continuously form and disappear. To address how this dynamical state terminates using simulations can be computationally challenging, especially for large systems. To circumvent this limitation, we treat the number of spiral waves as a stochastic population with a corresponding birth-death equation and use techniques from statistical physics to determine the mean episode duration of SDC. Motivated by cardiac fibrillation, during which the heart's electrical activity becomes disorganized and shows fragmenting spiral waves, we use generic models of cardiac electrophysiology. We show that the duration can be computed in minimal computational time and that it depends exponentially on domain size. Therefore, the approach can result in efficient and accurate predictions of mean episode duration which may be extended to more complex geometries and models.

## I. INTRODUCTION

Spiral waves are generic solutions of spatially extended excitable systems. Under certain conditions, these spiral waves are unstable and break up, creating multiple, drifting spiral waves. The resulting dynamical state can be described as spiral defect chaos (SDC), present in a variety of different pattern-forming systems [1–9]. During SDC, spiral waves continuously break down to form new ones, and are removed through collisions with other spiral waves or with non-conducting boundaries. as has been shown by many computational studies. This stochastic competition between creation and annihilation persists until the last spiral wave is terminated, with its duration representing a stochastic event. Often, the mean episode duration  $\tau$  of SDC is of interest, which is a statistical measure of the average until termination. Determining  $\tau$  through direct simulations of spatially extended models of SDC can be challenging because a statistically significant quantification of this stochastic quantity requires the time-consuming task of simulating a multitude of episodes [10, 11]. This becomes even more problematic for large geometry sizes since  $\tau$  typically increases as a function of the system size.

In this study, we will use generic excitable systems as an example and show how statistical physics techniques can be used to determine  $\tau$ . Specifically, we are motivated by cardiac fibrillation and use two cardiac electrophysiological models. During fibrillation, spiral waves underly the irregular conduction patterns and many computational studies have reported that the number of spiral waves increase due to wave break or decrease due to collisions with other spiral waves or with non-conducting boundaries [12–16]. In other words, this fibrillatory state can be described by SDC and lasts until the last spiral wave is terminated.

In this study we are interested in the mean episode duration  $\tau$  which is a statistical measure of the average time of annihilation of all spiral waves. Determining  $\tau$  through direct simulations of spatially extended cardiac models is challenging because previous simulation studies have shown that  $\tau$  increases sharply as a function of the system size [17, 18]. This increase is related to the so-called critical mass hypothesis which posits that fibrillation requires hearts with a minimal size [19, 20].

Our method to compute  $\tau$  treats number of spiral tips  $n$  as a stochastic quantity and casts its birth-death process into a master equation, a commonly used approach in the field of population dynamics [21–23]. This approach was also used previously for understanding

spiral wave dynamics in spatially extended fluid dynamical systems [1–9]. Furthermore, it was used in recent studies that examined filament turbulence in phenomenological models and that described the dynamics of surface defects in terms of a master equation [24–26]. Contrary to these studies, we focus here on tips migrating in 2D and on termination events and the associated mean episode duration. In our case, the master equation describes the probability  $P(n, t)$  of having  $n$  spiral tips at time  $t$  as

$$\frac{dP(n, t)}{dt} = \sum_r [W_r(n - r)P(n - r, t) - W_r(n)P(n, t)] \quad (1)$$

where  $W_r$  are transition rates for the number of spiral tips to change by  $r$  tips and can be computed directly from spatially extended simulations of cardiac models. Since tips are created and annihilated either as pairs or as singlets, we only need to consider  $r = \pm 1, \pm 2$ . As a boundary condition we take  $n = 0$  to be absorbing. This means that there is no escape from the no-tip state and that all birth rates for  $n = 0$  vanish:  $W_r(0) = 0$ . Furthermore, an additional boundary condition stems from the fact that for  $n = 1$  the pair-wise death rate equals 0:  $W_{-2}(1) = 0$ . Once the rates are known, we can construct a transition matrix which can be used to compute  $\tau$  at minimal computational cost [27].

For large  $n$ , the death rate will exceed the birth rate since tips will have a high probability of colliding. As a result, the number of spiral tips does not grow to very large numbers. If for small  $n$  the birth rate is larger than the death rate, then a long-lived (quasi-stationary) metastable state exists with a mean number of tips  $\bar{n}$ . The distribution associated with this metastable state is called the quasi-stationary distribution  $P_{qs}(n)$  [28, 29]. Note that for systems with an absorbing state at  $n = 0$ , the stationary distribution trivially corresponds to  $P(n) = 0$  for all  $n \neq 0$  and  $P(0) = 1$ . In the quasi-stationary state, the number of tips fluctuates around the average value for prolonged periods of time and the mean episode duration can be computed using

$$\frac{1}{\tau} = \sum_{r < 0} W_r(-r)P_{qs}(-r). \quad (2)$$

Termination only occurs during rare escape events, corresponding to a large fluctuation away from the mean number of tips. As a consequence, standard equilibrium statistical physics approaches based on small fluctuations do not apply [29, 30]. Instead, techniques from non-equilibrium statistical physics must be invoked to determine statistical quantities corresponding to extinction, including  $\tau$ .

To illustrate our stochastic approach to quantifying termination dynamics, we carry out simulations of SDC using spatially extended electrophysiological models. We should stress, however, that the approach should also work for other systems that exhibit spiral wave dynamics, including the complex Ginzburg-Landau equation [31] or simple phenomenological models [32]. The “direct” simulations use the standard reaction-diffusion equation:

$$\partial_t V = D \nabla^2 V - I_{ion}/C_m \quad (3)$$

where  $V$  is the transmembrane potential,  $C_m$  ( $\mu\text{F cm}^{-2}$ ) is the membrane capacitance and  $D \nabla^2$  expresses the inter-cellular coupling via gap junctions and diffusion constant  $D$ . The membrane currents in the electrophysiological model are denoted by  $I_{ion}$  which are governed by nonlinear evolution equations coupled to  $V$ . For our purposes, the precise form of  $I_{ion}$  is not important and we present results using the detailed Luo-Rudy (LR) model [33], modified to obtain spiral wave break-up as described in Qu *et al.* [34]. To stress the generality of our approach we also carry out simulations using the simplified Fenton-Karma (FK) model (parameter set 8) [35]. We perform the simulations in square two-dimensional computational domains although our approach can be equally well applied in more complex geometries. As boundary conditions, we consider both non-conducting and periodic boundary conditions, and we vary the area of the computational domain, which is equivalent to varying  $D$  while keeping the area constant. For both models, we use  $C_m = 1 \mu\text{F/cm}^2$  while the diffusion constant is chosen to be  $D = 0.0005 \text{ cm}^2/\text{ms}$  for the LR model and  $D = 0.001 \text{ cm}^2/\text{ms}$  for the FK model. Simulations are carried out with a discretization of  $0.025 \text{ cm}$ , using a 5-point stencil, and a time step of  $0.025 \text{ ms}$ , using explicit Euler integration. For both models, the conduction velocity along a cable is within the electrophysiological range:  $33 \text{ cm/s}$  for the LR model and  $51 \text{ cm/s}$  for the FK model. Errors in direct simulation results are reported as standard deviations.

## II. RESULTS USING DIRECT SIMULATIONS

Starting with a random initial condition that contains multiple spiral waves, we solve the reaction-diffusion equation and keep track of the number of spiral tips using a standard algorithm (Fig. 1A) [35]. The number of tips fluctuates and the simulation ends after time  $T_e$  when the number of spiral tips reaches 0 (Fig. 1B). We can compute the distribution of

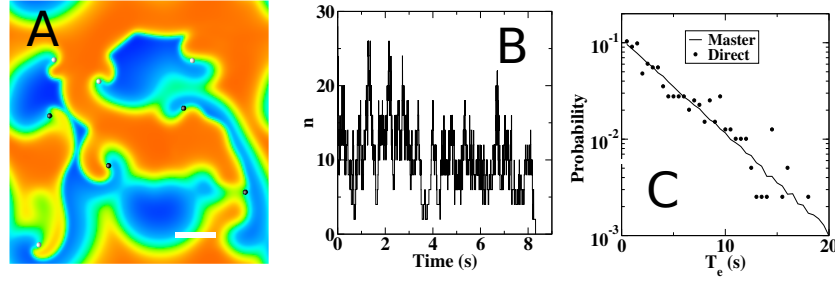


FIG. 1. **Direct numerical simulations provide statistics of spiral tip dynamics.** **A:** Snapshot of a simulation of the LR model in a  $7.5 \times 7.5$  cm computational domain with periodic boundary conditions. The voltage is represented using a color code with red (blue) corresponding to depolarized (repolarized) tissue. The location of the tips of counter- and clockwise rotation spiral waves are shown in black and white, respectively. (scale bar: 1cm) **B:** Typical time trace of the number of spiral tip pairs. For this particular simulation, spiral tips spontaneously extinguished after 8.3 s. **C:** Distribution of termination times for the direct simulations (symbols, computed using 400 termination events) and the master equation (solid line, computed using 10000 termination events).

these termination times by repeating the simulations many times, starting with different and independent initial conditions. These conditions are created by perturbing multi-spiral states with randomly placed current stimuli in the form of a current stimulus of duration 2 ms and strength several times the excitation threshold. After perturbation, the system is allowed to evolve for another 100 ms before measurements are started. Our simulations reveal that this distribution is exponentially distributed, indicating that spiral wave termination can be well described as a Poisson process (Fig. 1C).

Next, we compute the birth and death rates as a function of the number of tips  $n$  using different domain sizes with non-conducting boundaries by quantifying the number of transitions per time interval. The results are presented for the LR model in Fig. 2A-D. The number of transitions observed in the simulations depends on the domain size and on  $n$  and no transitions are recorded above some critical value of  $n$ . Here, to increase accuracy, we only consider rates that are determined using at least 100 transitions in the simulation. As a consequence, rates are computed up to a certain maximum value of  $n$ . In addition, for increasing domain sizes, transitions for small  $n$  become increasingly rare. As a result, in

large domains, the number of recorded transitions for small values of  $n$  may not reach 100. The rates corresponding to these values of  $n$  are therefore not included.

Examining the computed rates, we see that  $W_{-1}$  depends linearly on the number of spiral tips for all domain sizes (Fig. 2A). The remaining rates, however, show a more complex dependence on the number of tips, indicating the existence of non-trivial long-range interactions between spiral tips (Fig. 2B-D). As a result, the rate curves are not easily fit by simple power laws. Therefore, we employ a smoothing spline fit to the data to determine rates corresponding to transition events with less than the minimum number. Note that this interpolation takes into account the zero rate for either  $n = 1$  (periodic boundary conditions) or  $n = 0$  (non-conducting boundaries).

In addition, we compute the rates for the FK model. The results, presented in Fig. 3, show the same linear dependence of  $W_{-1}$  on the number of spiral tips, along with a more complex dependence of the other rates. We can also compute the  $W_{\pm 2}$  rates for domains that contain periodic boundary conditions. The results of these simulations are shown in Fig. 4 for both models and are qualitatively similar to the results presented in Fig. 2 and 3. As a consistency check, we can use these rates to compute the distribution of termination times. As expected, this distribution is exponential and agrees well with the one computed using direct simulations (Fig. 1C).

Importantly, we find that at large  $A$  all rates collapse onto a single curve when plotted as a function of the density  $q = n/A$ . Specifically, the  $W_{\pm 2}$  rates are found to scale with the area as  $W_{\pm 2}(n) \sim Aw_{\pm 2}(q)$  (Figs. 2F, 3F, and 4C, F), indicating that the birth and death rates only depend on the density and that tips are well-mixed. Furthermore, the  $W_{\pm 1}$  rates scale with the perimeter  $L$  as  $W_{\pm 1}(n) \sim Lw_{\pm 1}(q)$  (Figs. 2E and 3E). Here, and in the following, we will take the continuum limit such that  $q$  and functions that depend on this variable are considered to be continuous. Note that this observed linear scaling of  $W_{-1}$  with  $L$  implies that the death rate is proportional with the length of the non-conducting boundary and that creating ablation lesions will increase this rate. Furthermore, such scaling is expected if single tips annihilate through simple collision processes and get created near the boundaries.

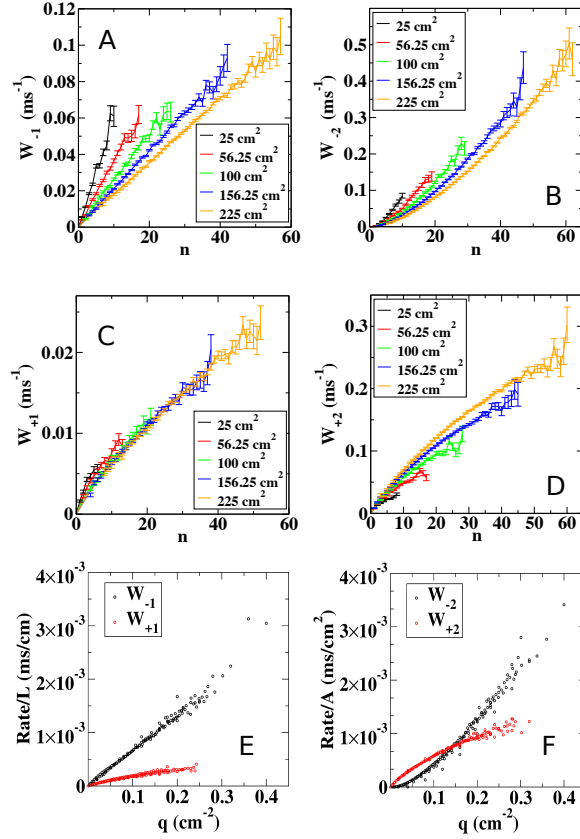


FIG. 2. Transition rates for the LR model computed using direct simulations and non-conducting boundaries. **A-D**: The birth and death rates for  $n \rightarrow n - 1$  (A),  $n \rightarrow n - 2$  (B),  $n \rightarrow n + 1$  (C),  $n \rightarrow n + 2$  (D) computed in a square geometry of various sizes. Error bars represent standard deviation. **E**: The  $W_{\pm 1}$  rates, normalized by the perimeter of the domain, as a function of the density of tips,  $q = n/A$ . **F**: The  $W_{\pm 2}$  rates, normalized by the area of the domain, as a function of the density of tips.

### III. RESULTS USING TRANSITION RATES

Once the transition rates are determined, it is straightforward to compute the quasi-stationary distribution  $P_{qs}(n)$  using the transition matrix at minimal computational cost (Fig. 5A, B, D, and E) [27]. For small domains, this can be carried out using the rates obtained in the simulations while for larger domains, where the rates for small  $n$  cannot be computed accurately, we can use the interpolated rates. As the domain size increases, the distribution shifts to larger values of  $n$ , and becomes more symmetric around its peak. Of



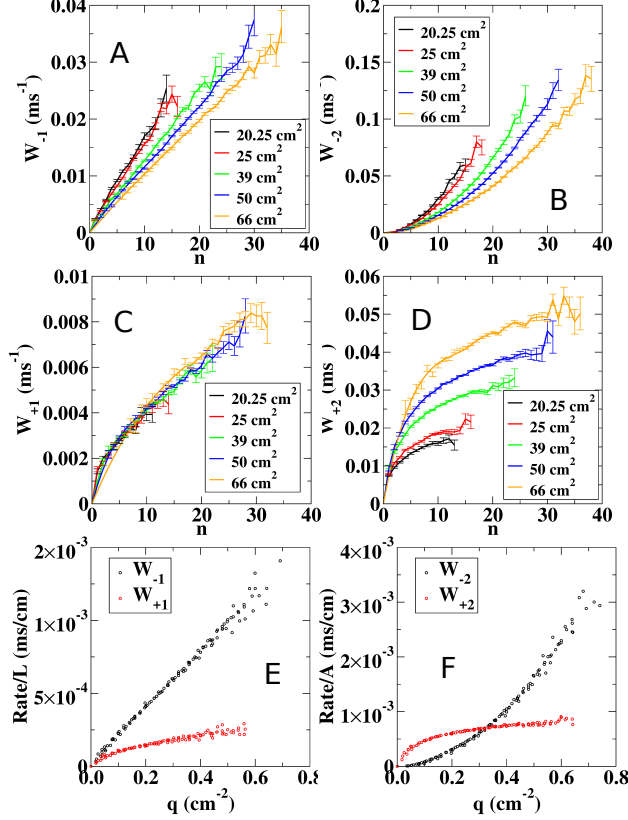


FIG. 3. **Transition rates for the FK model computed using direct simulations and non-conducting boundaries.** **A-D:** The birth and death rates for  $n \rightarrow n - 1$  (A),  $n \rightarrow n - 2$  (B),  $n \rightarrow n + 1$  (C),  $n \rightarrow n + 2$  (D) computed in a square geometry of various sizes. Error bars represent standard deviation. **E:** The  $W_{\pm 1}$  rates, normalized by the perimeter of the domain, as a function of the density of tips,  $q = n/A$ . **F:** The  $W_{\pm 2}$  rates, normalized by the area of the domain, as a function of the density of tips.

course, the quasi-stationary distribution computed using the transition matrix agrees very well with the one determined using direction simulations. This agreement is shown for the largest domain size in Fig. 5A, B, D, and E (symbols) but is also valid for other domain sizes. The average number of tips,  $\bar{n}$ , increases with system size and our simulations reveal that it depends linearly on the area of the computational domain for both boundary conditions (Fig. 5C and F).

For geometries that do not contain any non-conducting boundaries it is possible to derive closed-form solutions for the quasi-stationary distribution. In this case,  $n$  is always even and tips will be created and annihilated in pairs such that  $W_{\pm 1} = 0$ . The quasi-stationary

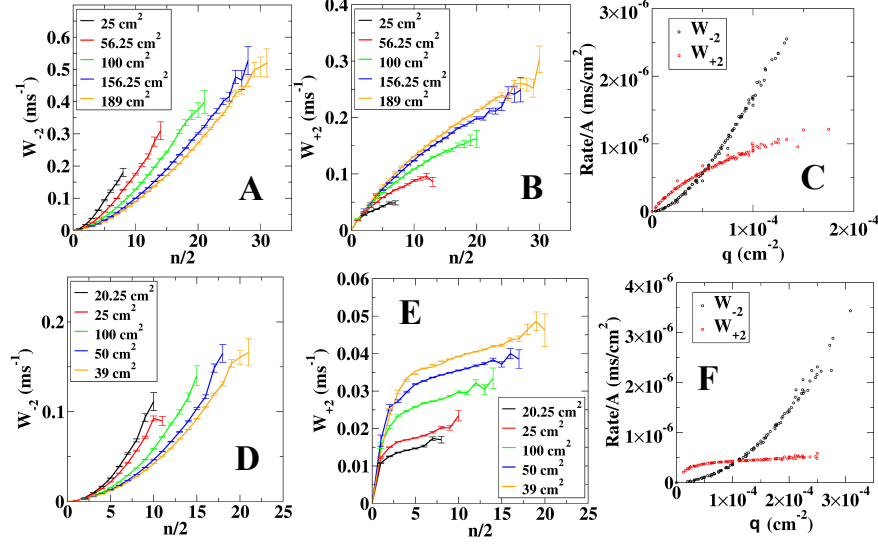


FIG. 4. **Transition rates for the LR (A-C) and FK model (D-F) computed using direct simulations with periodic boundary conditions.** **A, B and D, E:** The birth and death rates for  $n \rightarrow n - 2$  (A, D),  $n \rightarrow n + 2$  (B, E) computed in a square geometry of various sizes with absorbing boundaries. Error bars represent standard deviation. **C and F.** The  $W_{\pm 2}$  rates, normalized by the area of the domain, as a function of the density of tips.

distribution can be obtained by setting the left hand side in Eq. 1 to zero, resulting in the recursion relationship

$$P_{qs}(n) = P_{qs}(0) \prod_{j=2}^n W_{+2}(2j-2)/W_{-2}(2j) \quad (4)$$

where  $P_{qs}(0)$  can be determined by the normalization condition  $\sum_{n=0}^{\infty} P_{qs}(n) = 1$  [23].

The deterministic equation corresponding to the master equation can be found in a straightforward manner [23]:

$$\frac{dn}{dt} = 2W_{+2}(n) - 2W_{-2}(n) \quad (5)$$

As a consequence, the deterministic stationary state is determined by  $W_{+2}(n^*) = W_{-2}(n^*)$ . The maximum value of the quasi-stationary distribution occurs for  $P_{qs}(n-2)/P_{qs}(n) \approx 1$ , corresponding to  $W_{+2}(\bar{n}-2) = W_{-2}(\bar{n})$ . Therefore, for large values of  $A$  the stochastic average number can be well approximated by the deterministic average number,  $\bar{n} \approx n^*$ . Furthermore, using our numerically found scaling, we obtain  $w_{+2}(q^*) = w_{-2}(q^*)$ , where  $q^* = n^*/A$ . Hence, the average density is independent of the area and  $n^*$ , and thus  $\bar{n}$ ,

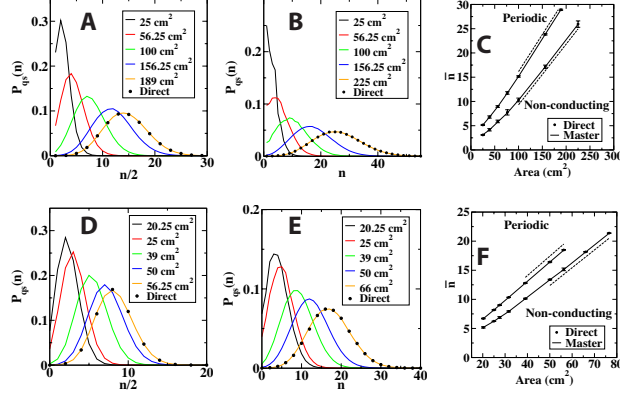


FIG. 5. **Dependence of spiral tip dynamics on the domain size for LR model (A-C) and the FK model (D-F).** **A, B and D, E:** The quasi-stationary distribution for periodic (A, D) and non-conducting boundary conditions (B, E) using different domain sizes as computed using the transition matrix. The symbols show the quasi-stationary distribution as computed using the direct simulations. **C, F:** The average number of tips as a function of the area of the computational domain, computed using direct simulations (symbols) and using the master equation approach (line). The dashed curves are straight lines.

scale with  $A$ , consistent with the scaling found in the simulations (Fig. 5C and F). For domains that contain non-conducting boundaries, the  $\pm 1$  rates are no longer zero and the corresponding deterministic equation reads

$$\frac{dn}{dt} = 2W_{+2}(n) - 2W_{-2}(n) + W_{+1}(n) - W_{-1}(n). \quad (6)$$

Using our obtained scaling, we have for the deterministic stationary state:

$$2w_{+2}(q^*) - 2w_{-2}(q^*) + w_{+1}(q^*)/\sqrt{A} - w_{-1}(q^*)/\sqrt{A} = 0 \quad (7)$$

For large areas, the last two terms can be neglected and the average number of tips will again scale linearly with the area.

#### IV. MEAN EPISODE DURATION

To find the mean episode duration  $\tau$  in the direct simulations, we average the termination times  $T_e$  obtained from each independent simulation. This computation becomes more and more time consuming as  $A$  increases since termination becomes less and less likely. As a

consequence, the number of determined termination events we consider vary from 400 for small domains to less than 10 for the largest areas still amenable to direct simulations. Our results reveal that  $\tau$  increases sharply as the domain size becomes larger, consistent with earlier computational studies [18]. More specifically,  $\tau$  displays an exponential dependence on the size of the domain, both for periodic and non-conducting boundary conditions (red symbols, Fig. 6), a result that agrees with the earlier study by Qu [17].

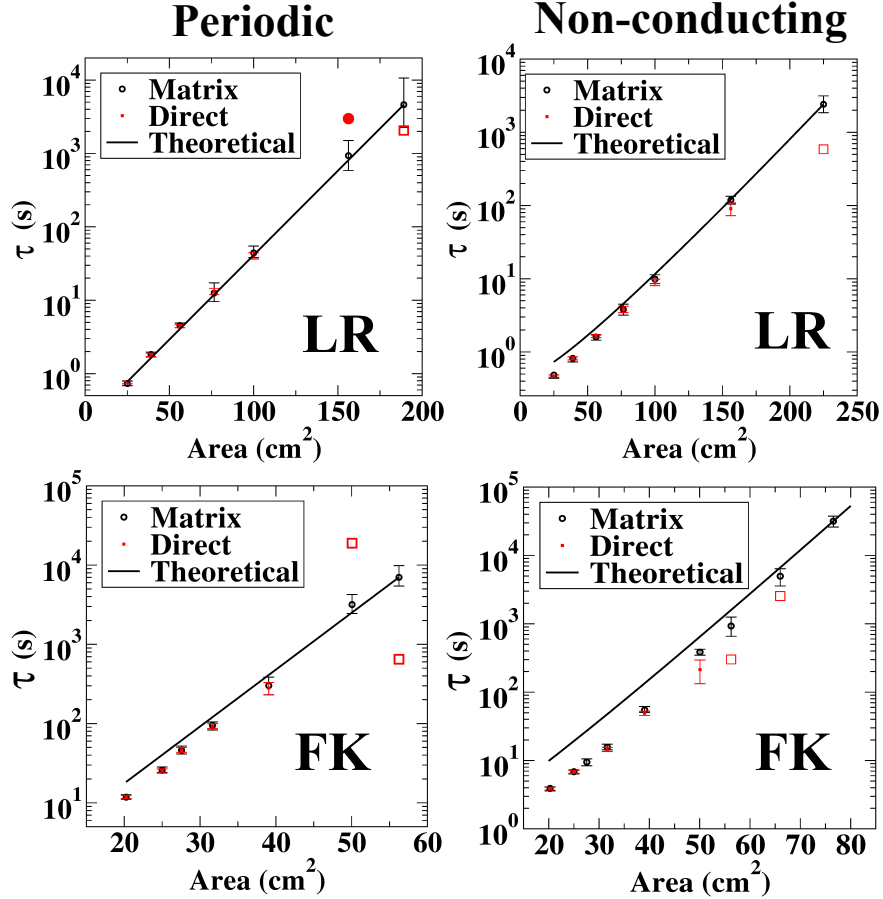


FIG. 6. Termination times as a function of the system size for the LR model (upper row) and FK model (lower row). Red symbols show  $\tau$  as a function of the area of the computational domain from direct simulations using domains with periodic boundary conditions (left column) and non-conducting boundaries (right column). Also shown are the results from the master equation approach (black symbols) and from the closed-form expression obtained using the WKB analysis (solid line). The red square represents the result of a single termination event computed using direct simulations while the solid red circle represents the computed time for a single computation that did not result in a termination.

Rather than using direct simulations to determine an average value for  $T_e$ , it is straightforward to use the interpolated transitions rates and the resulting transition matrix to compute  $\tau$  using simple matrix operations [27]. For this, we construct a transition matrix  $Q$  for all transient states  $n > 0$ , with elements  $Q_{ij}$  representing the probability of transitioning from state  $i$  to state  $j$ . The probability of reaching state  $j$  from state  $i$  in  $t$  steps is then given by the  $ij^{th}$  entry of  $Q^t$ . Summing this over all time results in the so-called fundamental matrix  $N = I + Q + Q^2 + \dots = (I - Q)^{-1}$ , where  $I$  is the identity matrix. Each element of the fundamental matrix  $N_{ij}$  represents the mean duration our system will spend in state  $j$  given an initial state  $i$ , which can be used to determine the quasi-stationary distribution. Moreover the mean time to extinction  $\tau$  is given by  $N\vec{e}$ , where  $\vec{e}$  is a column vector of ones. The confidence intervals for  $\tau$  are computed through bootstrapping as follows. First we re-sample each transition rate by drawing a value from a binomial distribution with probability equal to the original transition rate and using the number of recorded transitions from the direct simulation. We then proceed by interpolating these resampled transition rates and computing  $\tau$  from these interpolated transition rates. This is computed for 1000 trials and the confidence interval is determined from the 5th to the 95th percentile of the resulting  $\tau$  across all trials.

The resulting values for  $\tau$  agree well with the direct numerical simulations (black symbols, Fig. 6). Importantly, using the transition matrix allows us to estimate the mean episode duration for system sizes where determination of mean episode duration with direct simulations is impossible. For example, directly simulating a single extinction event on a domain with area  $A = 225\mu m^2$  and non-conducting boundaries was found to take approximately 100 hours of CPU time. Estimating  $\tau$  from this single event is not useful as the error is large and generating a sufficient amount of termination events is not practical. Furthermore, for other larger domain sizes our direct simulations failed to produce a single termination event, even after 7 days of CPU time. Using the interpolated transition rates computed from this single, non-terminating event, however, we are still able to use the transition matrix (Fig. 6) to predict the mean episode duration. Moreover,  $\tau$  can already be estimated using only a fraction of the data, and thus simulation time, further demonstrating the power of the approach. This is shown in Fig. 7 where we plot  $\tau$  as a function of the fraction of computational data from a direct simulation of the LR model. Obviously, for larger fractions, the errors in the transition rates become smaller, resulting in smaller confidence intervals.

Furthermore, the mean termination time converges as the fraction increases and can be reasonably well estimated from a small fraction of the entire dataset.

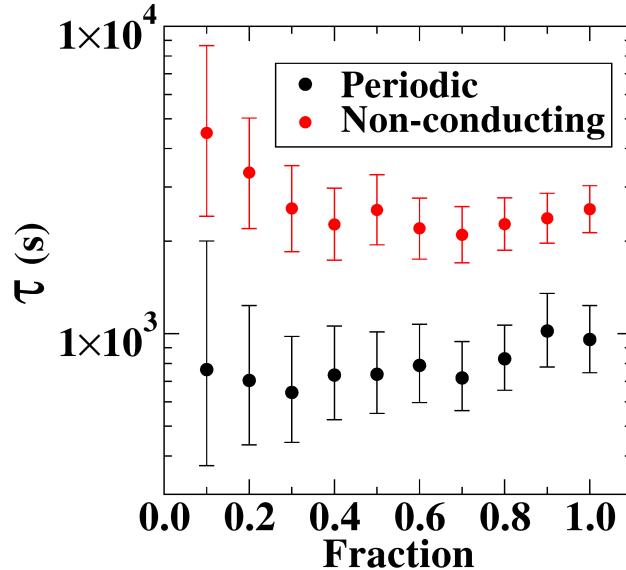


FIG. 7. **Accuracy of the master equation approach.** The mean episode duration computed using the master equation as a function of the fraction of computational data obtained using direct simulations of the LR model. Data segments of size indicated by fraction were started at random positions. Results are shown for  $A = 225\text{cm}^2$  for the non-conducting case and for  $A = 189.0625\text{cm}^2$  for the periodic case. The error bars are determined using bootstrapping and represent the 5% and 95% confidence interval.

## V. SCALING RESULTS

We can also use our stochastic analysis of termination to determine the scaling of  $\tau$  with the area. For periodic boundary conditions, it is possible to obtain an analytical expression for  $\tau$  [23]:

$$\tau(n_0) = \sum_{k=1}^{n_0/2} \phi(2(k-1)) \sum_{j=k}^{\infty} \frac{1}{\phi(2j)W_{+2}(2j)} \quad (8)$$

where  $n_0$  is the initial number of spiral tips,  $\phi(k) = \prod_{i=1}^{k/2} W_{-2}(2i)/W_{+2}(2i)$ , and  $\phi(0) \equiv 1$ . Using the numerically determined rates we find that  $\tau$  quickly converges as  $n_0$  becomes large and that  $\tau(\bar{n})$  agrees well with the values obtained using the numerical methods. This is

shown explicitly in Fig. 8 which plots the mean episode duration as a function of the initial number of tips for one particular domain size. We have verified that qualitatively similar results hold for other domain sizes.

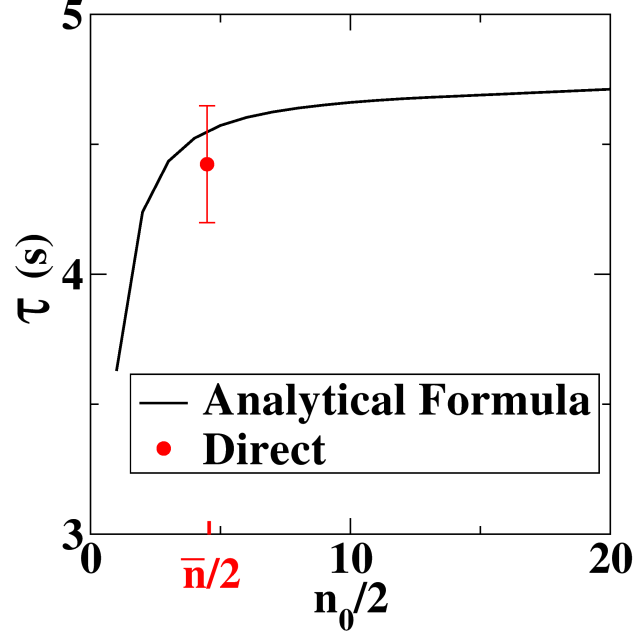


FIG. 8. **Analytical formula for periodic boundary conditions.** Mean episode duration  $\tau$  as computed using the analytical formula in the main text as a function of the initial number of tips,  $n_0$ . Symbol corresponds to the result from direct simulations ( $\bar{n} \approx 9$ ). Results are shown for the LR, using a domain of size 7.5cmx7.5cm.

To determine the scaling with the area we focus on the first term of this expression,  $\tau(2) = \sum_{j=1}^{\infty} (\phi(2j)W_{+2}(2j))^{-1}$ . We can write  $\phi(2j)$  as

$$\ln[\phi(2j)] = \sum_{z=1}^j \ln \left[ \frac{W_{-2}(2z)}{W_{+2}(2z)} \right] \approx -\frac{A}{2} \int_{2/A}^x \ln \frac{w_{+2}(s)}{w_{-2}(s)} ds \quad (9)$$

where we have used the fact that the transition rates scale with the area  $A$  and have defined  $s = 2z/A$  and  $x = 2j/A$ . As a result, the mean episode duration becomes

$$\tau \approx \int_0^{\infty} \frac{\exp \left[ A \int_{2/A}^x \ln \sqrt{\frac{w_{+2}(s)}{w_{-2}(s)}} ds \right]}{2w_{+2}(x)} dx. \quad (10)$$

For large  $A$ , this integral will be sharply peaked around  $q^*$ . Thus,  $\tau$  has the following scaling behavior [36]:

$$\tau \sim \exp \left[ A \int_{2/A}^{q^*} \ln \sqrt{\frac{w_{+2}(s)}{w_{-2}(s)}} ds \right] \quad (11)$$

and, as an immediate consequence of the observed scaling of the transition rates, we find that  $\tau$  scales exponentially with the area, consistent with our direct numerical results (Fig. 6).

We can also use approximation methods to determine the scaling of the mean episode duration by viewing the number of spiral tips as a stochastic population in a metastable state. This approach is particularly useful for domains containing non-conducting boundaries, for which it is no longer possible to derive an exact expression for  $\tau$ . As long as  $A$ , equivalent to the total population size in models of population biology, is sufficiently large, we can use a dissipative WKB approximation, pioneered by Kubo et al. [37]. In this approximation, the quasi-stationary distribution is assumed to obey  $P_{qs}(q) \sim e^{-AS(q)}$  where  $S(q)$  is a function called the action. We can now use our obtained scaling  $W_r(n) = A^{r/2}w_r(q)$ , together with the assumed form of  $P_{qs}(q)$ , and substitute them into the stationary form of Eq. 1. This equation is written in terms of the continuous rescaled variable  $q = n/A$  so that  $n - r \rightarrow q - r/A$  [29]. For the periodic case, we take  $S(q) = S_0(q) + O(A^{-1})$  while for absorbing boundaries, since the scaling of the  $\pm 1$  rates goes as  $\sqrt{A}$  while the  $\pm 2$  rates go as  $A$ , we use  $S(q) = S_0(q) + A^{-1/2}S_1(q) + O(A^{-1})$ . The resulting equation can then be expanded in terms of  $1/A$  which yields, to  $O(1)$ , a Hamilton-Jacobi equation

$$H(q, p) = \sum_r A^{r/2} w_r(q) (e^{rp} - 1) = 0 \quad (12)$$

where  $p(q) = \partial S / \partial q$  is the fluctuation momentum [28, 29].

From the Hamiltonian  $H$  we can define the dynamics of  $p$  and  $q$  using  $\frac{dp}{dt} = -\frac{\partial H}{\partial q}$  and  $\frac{dq}{dt} = \frac{\partial H}{\partial p}$ . The non-trivial solution of  $H(q, p_a(q)) = 0$  corresponds to the activation trajectory in the  $q, p$  phase space [28–30, 37, 38]. This trajectory describes the most probable path along which the system evolves from the metastable state  $(q^*, 0)$  to a point  $q$  in phase space. Since we are interested in extinction, we will consider the trajectory that connects  $(q^*, 0)$  with  $[0, p(0)]$ , the so-called “optimal” path to extinction [28]. This  $q, p$  phase space, along with the activation trajectory, is shown in Fig. 9 for periodic boundaries for both the LR and the FK model. The optimal path can be determined numerically but can also be determined using approximate closed-form relations. Specifically, for periodic boundary conditions, we find

$$S_0 = \int_{q^*}^{2/A} \ln \gamma_0 dq, \quad (13)$$



and  $\gamma_0 = \sqrt{\frac{w-2}{w+2}}$ . In Fig. 9, this corresponds to the area between the activation trajectory and the  $q$  axis, represented by the shaded part. Thus, we find that the mean episode duration scales as  $\tau \sim e^{AS_0}$ , consistent with Eq. 11. For absorbing boundaries, we can solve for  $S_1$  perturbatively, yielding

$$S_1 = \int_{q^*}^{2/A} \frac{(\gamma_0 w_{+1} - w_{-1})(\gamma_0 - 1)}{2\gamma_0(w_{+2} - w_{-2})} dq. \quad (14)$$

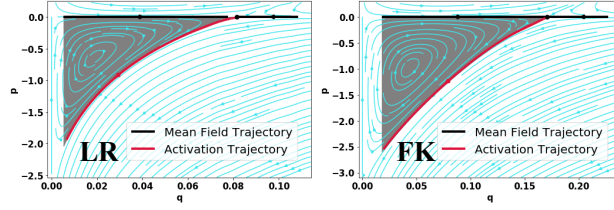


FIG. 9. **WKB approach to spiral tip dynamics.** Phase portrait of the Hamiltonian dynamics in  $q, p$  space for periodic boundary conditions in the LR and FK model, showing the activation trajectory of the WKB Hamiltonian (red line). The shaded area represents the exponential factor  $S_0$ .

Using our formulation, we can now compute the mean episode duration for any system size once the rates for a single domain  $\hat{A}$  are determined. Specifically, after computing for this particular domain both  $\hat{S}_0$  and  $\hat{S}_1$  and the corresponding mean episode duration  $\hat{\tau}$ , we can find  $\tau$  as a function of the system size using:

$$\tau(A) \approx \hat{\tau} e^{(A-\hat{A})\hat{S}_0 + (\sqrt{A}-\sqrt{\hat{A}})\hat{S}_1}. \quad (15)$$

This scaling law for  $\tau$  agrees well with the values of  $\tau$  computed from the master equation, especially for larger values of  $A$  (Fig. 6), justifying the WKB approximation. For these larger domain sizes, the factors  $S_0$  and  $S_1$  converge, making the estimate from Eq. 15 to be more accurate, as shown in Fig. 10A. This is consistent with the obtained quasi-stationary distributions which become more symmetric around their peak value for larger domain size (Fig. 5), rendering the WKB approximation more accurate. Furthermore, as is the case for  $\tau$  (Fig. 7), both  $S_0$  and  $S_1$  can be estimated using the interpolated rates and only a fraction of the direct simulation data (Fig. 10B). Thus, accurate estimates for arbitrary domain sizes do not require simulating actual termination events. Finally, the exponential scaling of  $\tau$  with system size  $A$  reveals that, even though spiral wave driven fibrillation

will always terminate, its mean episode duration depends critically on the size of the heart. Of course, this result is valid as long as the specifics of the model do not change. Other factors, including changes in electrophysiological parameters, can have an effect of mean termination duration. For large values of  $A$ ,  $\tau$  can be large while for very small values of  $A$  as found, for example, in rodents, the mean episode duration will be well below 1 s. These findings are fully consistent with the well-established critical mass hypothesis which posits that fibrillation only occurs in hearts of a minimum size [17, 19, 20].

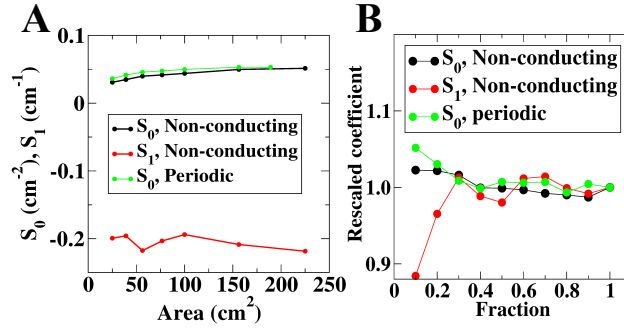


FIG. 10. **WKB parameters as a function of area size for the LR model** A: The exponential coefficients  $S_0$  and  $S_1$  as a function of domain size for periodic and non-conducting boundaries. B: The exponential factors  $S_0$  and  $S_1$ , rescaled by their value computed at the largest computational data set, as a function of the fraction of computational data obtained using direct simulations. Data segments of size indicated by fraction were started at random positions. Shown are the results for  $A = 225\text{cm}^2$  for the non-conducting case and for  $A = 189.0625\text{cm}^2$  for the periodic case.

## VI. SUMMARY

In summary, we present a statistical approach to quantify spiral wave dynamics in spatially extended domains. This approach recasts the problem into a master equation, after which statistical physics methods can be employed. Our approach is valid for any model exhibiting SDC. Key in this approach are the transition rates, which were computed numerically from a limited set of direct simulations. Using a dissipative WKB approach, we find that the mean episode duration of SDC can be computed in minimal computational time. In addition, we show that this duration depends exponentially on domain size.

Our results should be generally applicable to any system exhibiting SDC. Here we have

used electrophysiological models, motivated by the spiral wave dynamics observed during fibrillation when the heart’s electrical activity becomes disorganized [12, 39–41]. Clearly, our fibrillation model is an idealized and simplified version of the clinical reality since the heart is a heterogeneous 3D object. Nevertheless, it is intriguing to note that the exponential dependence of the mean episode duration is consistent with the critical mass hypothesis which states that fibrillation requires a minimal organ size [17, 19]. Furthermore, some of the simplifications of the current model might be overcome by future extensions. First, our approach should also be applicable to more complex, realistic geometries. Geometry data are routinely obtained in patients and electrophysiological models can be readily implemented using computational tools. This should allow us to compute rate equations in realistic geometries, after which we can use the same approach as detailed here. This extension might also be used to study the effect of different surgically created lesion sets and pharmacological interventions on the termination time and has the potential to be an important step towards determining optimal therapeutic interventions aimed at minimizing the duration of fibrillation episodes. Second, we may be able to extend the model to include tissue inhomogeneities. As long as the spiral wave is not trapped, one should be able to compute the creation and annihilation rates as carried out in this study. Third, the approach can be extended to include tissue with a non-zero thickness, appropriate for the ventricles and possibly for atrial tissue. To extend our approach to this type of problem we will need to track spiral wave tips on both surfaces. In addition, it would be interesting to further study the dependence of the rates on the number of tips. If, for example, rational functions for these rates can be derived, it should be possible to obtain analytical expressions for  $\tau$ . Finally, it would be interesting to compare scaling of fibrillation in healthy and diseased hearts by simulating appropriate electrophysiological models.

## VII. ACKNOWLEDGEMENTS

We thank Brian A. Camley and David A. Kessler for valuable suggestions. We gratefully acknowledge support from the National Institutes of Health (R01 HL122384) and the

- [1] P. Coulet, L. Gil, and J. Lega, Physical Review Letters **62**, 1619 (1989).
- [2] I. Rehberg, S. Rasenat, and V. Steinberg, Physical Review Letters **62**, 756 (1989).
- [3] R. E. Ecke, Y. Hu, R. Mainieri, and G. Ahlers, Science **269**, 1704 (1995).
- [4] M. Hildebrand, M. Bär, and M. Eiswirth, Physical Review Letters **75**, 1503 (1995).
- [5] Q. Ouyang and J.-M. Flesselles, Nature **379**, 143 (1996).
- [6] D. A. Egolf, I. V. Melnikov, W. Pesch, and R. E. Ecke, Nature **404**, 733 (2000).
- [7] K. E. Daniels and E. Bodenschatz, Physical Review Letters **88**, 034501 (2002).
- [8] H. Varela, C. Beta, A. Bonnefont, and K. Krischer, Physical Review Letters **94**, 174104 (2005).
- [9] C. Beta, A. S. Mikhailov, H. H. Rotermund, and G. Ertl, EPL (Europhysics Letters) **75**, 868 (2006).
- [10] N. Virag, V. Jacquemet, C. Henriquez, S. Zozor, O. Blanc, J.-M. Vesin, E. Pruvot, and L. Kappenberger, Chaos: An Interdisciplinary Journal of Nonlinear Science **12**, 754 (2002).
- [11] O. Dossel, M. W. Krueger, F. M. Weber, M. Wilhelms, and G. Seemann, Med Biol Eng Comput **50**, 773 (2012).
- [12] A. Karma, Annu. Rev. Condens. Matter Phys. **4**, 313 (2013).
- [13] F. H. Fenton, E. M. Cherry, H. M. Hastings, and S. J. Evans, Chaos **12**, 852 (2002).
- [14] V. Zykov, A. Krekhov, and E. Bodenschatz, Proceedings of the National Academy of Sciences **114**, 1281 (2017).
- [15] M. Fink, S. A. Niederer, E. M. Cherry, F. H. Fenton, J. T. Koivumäki, G. Seemann, R. Thul, H. Zhang, F. B. Sachse, D. Beard, *et al.*, Progress in biophysics and molecular biology **104**, 2 (2011).
- [16] Z. Qu, J. N. Weiss, and A. Garfinkel, American Journal of Physiology-Heart and Circulatory Physiology **276**, H269 (1999).
- [17] Z. Qu, American Journal of Physiology-Heart and Circulatory Physiology **290**, H255 (2006).
- [18] S. Sinha, A. Pande, and R. Pandit, Physical Review Letters **86**, 3678 (2001).
- [19] W. E. Garrey, American Journal of Physiology–Legacy Content **33**, 397 (1914).

- [20] G. D. Byrd, S. M. Prasad, C. M. Ripplinger, T. R. Cassilly, R. B. Schuessler, J. P. Boineau, and R. J. Damiano, *Circulation* **112**, I (2005).
- [21] R. Lande, S. Engen, and B.-E. Saether, *Stochastic population dynamics in ecology and conservation* (Oxford University Press on Demand, 2003).
- [22] N. G. Van Kampen, *Stochastic processes in physics and chemistry*, Vol. 1 (Elsevier, 1992).
- [23] C. Gardiner, *Stochastic Methods: A Handbook for the Natural and Social Sciences* (Springer-Verlag, Berlin Heidelberg, 2009).
- [24] J. Davidsen, M. Zhan, and R. Kapral, *Physical Review Letters* **101**, 208302 (2008).
- [25] J. Reid, H. Chaté, and J. Davidsen, *EPL (Europhysics Letters)* **94**, 68003 (2011).
- [26] G. St-Yves and J. Davidsen, *Physical Review E* **91**, 032926 (2015).
- [27] M. Newman, *Networks; an introduction* (Oxford University, Oxford, 2010).
- [28] M. Dykman, E. Mori, J. Ross, and P. Hunt, *The Journal of chemical physics* **100**, 5735 (1994).
- [29] M. Assaf and B. Meerson, *Physical Review E* **81**, 021116 (2010).
- [30] C. R. Doering, K. V. Sargsyan, and L. M. Sander, *Multiscale Modeling & Simulation* **3**, 283 (2005).
- [31] I. S. Aranson and L. Kramer, *Reviews of Modern Physics* **74**, 99 (2002).
- [32] D. Barkley, M. Kness, and L. S. Tuckerman, *Physical Review A* **42**, 2489 (1990).
- [33] C. H. Luo and Y. Rudy, *Circ Res* **68**, 1501 (1991).
- [34] Z. Qu, F. Xie, A. Garfinkel, and J. N. Weiss, *Ann Biomed Eng* **28**, 755 (2000).
- [35] F. Fenton and A. Karma, *Chaos* **8**, 20 (1998).
- [36] P. L. Krapivsky, S. Redner, and E. Ben-Naim, *A kinetic view of statistical physics* (Cambridge University Press, 2010).
- [37] R. Kubo, K. Matsuo, and K. Kitahara, *Journal of Statistical Physics* **9**, 51 (1973).
- [38] D. A. Kessler and N. M. Shnerb, *Journal of Statistical Physics* **127**, 861 (2007).
- [39] J. Jalife, *Journal of cardiovascular electrophysiology* **14**, 776 (2003).
- [40] S. M. Narayan, D. E. Krummen, and W.-J. Rappel, *Journal of cardiovascular electrophysiology* **23**, 447 (2012).
- [41] S. M. Narayan, D. E. Krummen, M. W. Enyeart, and W.-J. Rappel, *PLoS ONE* **7**, e46034 (2012).